

GRAPHENE

Tunable excitons in bilayer graphene

Long Ju,^{1,2*} Lei Wang,^{1,2*} Ting Cao,³ Takashi Taniguchi,⁴ Kenji Watanabe,⁴ Steven G. Louie,^{3,5} Farhan Rana,⁶ Jiwoong Park,^{1,7} James Hone,^{8†} Feng Wang,^{3,5,9†} Paul L. McEuen^{1,2†}

Excitons, the bound states of an electron and a hole in a solid material, play a key role in the optical properties of insulators and semiconductors. Here, we report the observation of excitons in bilayer graphene (BLG) using photocurrent spectroscopy of high-quality BLG encapsulated in hexagonal boron nitride. We observed two prominent excitonic resonances with narrow line widths that are tunable from the mid-infrared to the terahertz range. These excitons obey optical selection rules distinct from those in conventional semiconductors and feature an electron pseudospin winding number of 2. An external magnetic field induces a large splitting of the valley excitons, corresponding to a g-factor of about 20. These findings open up opportunities to explore exciton physics with pseudospin texture in electrically tunable graphene systems.

Bilayer graphene (BLG) is a material with a continuously tunable bandgap (*1–5*) (Fig. 1A), a pseudospin winding number of 2 (*6–8*), and a valley-dependent Berry phase (*7*), providing a fertile ground to explore two-dimensional (2D) physics beyond conventional semiconductors. Excitons in BLG are predicted (*9, 10*) to have large binding energies and be distinct from those in conventional semiconductors because of their pseudospin texture. The optical transition energies for these excitons are expected to be tunable from the mid-infrared to the far-infrared (*1*), relevant for many scientific and technological applications such as molecular spectroscopy, materials analysis, thermal imaging, and astronomical applications (*11*). In particular, strong and *in situ* tunable exciton resonances with high quality factors in this range could enable the realization of tunable infrared detectors, light-emitting diodes and lasers, and the exploration of new physics.

Despite their fundamental and practical interest, BLG excitons have to date not been observed. Previous optical spectroscopy of BLG on SiO₂/Si substrates revealed the tunable bandgap in BLG (*7*) but did not observe any excitonic signatures because of the large inhomogeneous broadening caused by the SiO₂ substrates. In addition, conventional far-infrared absorption spectroscopy on ultraclean BLG has been challenging because of

limited sizes of hexagonal boron nitride (hBN)-encapsulated graphene samples (*12*).

Here, we report the observation of excitons in BLG using photocurrent spectroscopy of high-quality hBN-encapsulated (*12*) BLG devices (Fig. 1B). The BN-BLG-BN stack sits on a piece of graphite local back gate (BG), and a 14-nm layer of nickel/chrome alloy is deposited on top as the semitransparent top gate (TG). Source (S) and drain (D) electrodes are used to apply voltage bias and measure photocurrent generated in the device. Under infrared illumination, electron-hole pairs are generated in BLG (inset in Fig. 1F), and they lead to a significant photocurrent proportional to the optical absorption in the bilayer. Optical absorption spectra can be obtained by a modified Fourier transform infrared (FTIR) spectroscopy (Fig. 1D), where the BLG photocurrent signal as a function of the delay in the FTIR spectroscopy is recorded (*13, 14*). Figure 1E shows a typical photocurrent interferogram for bandgap-opened BLG. The corresponding spectrum in frequency domain is plotted in Fig. 1F. We observed two sharp absorption peaks, labeled P1 and P2 (red arrows), and a continuous smooth absorption above P2.

Figure 2A shows three normalized (*14*) photocurrent spectra taken at displacement fields of $D = 0.69, 1.03,$ and 1.37 V/nm , which are achieved by controlling the top and bottom gate voltages (*1, 5*). As the bandgap widens with increasing D , the two peaks P1 and P2 shift to higher energies. More spectra are shown in Fig. 2B as a 2D color plot, where we continuously tune the displacement field from 0.67 to 1.37 V/nm . The peaks P1 and P2 are clearly seen as the diagonal lines in the 2D plot. Spectra at even lower D are included in fig. S2. As shown in Fig. 2C, both P1 and P2 (red and black dots, respectively) follow a largely linear relation with D , but the ratio $(P2 - P1)/P2$ increases monotonically with decreasing D .

Figure 2D shows that both P1 and P2 can be well described by a single Lorentzian line shape (the high-energy side of P2 is affected by other optical resonances), with full width at half maximum (FWHM) of 0.4 and 1.3 meV , respectively.

The P1 line width is only half of the thermal energy $k_B T$ at 10 Kelvin , corresponding to a quality factor of up to ~ 250 . Both peaks are much narrower than optical resonances in other semiconductors (such as Hg_xCd_{1-x}Te) in this spectral range (*15*). Interestingly, above P2, all spectra converge to the same line, indicating that the absorption well above the field-induced bandgap approaches the absorption of a pristine BLG, which is $\sim 4\%$ at 120 meV (in suspended graphene) (*16, 17*). Using this as a reference, we found that the absorption at the P2 peak is about 20%.

The optical resonances at P1 and P2 could in principle originate from excitations of free electron-hole pairs, excitons, and/or impurity states. One possible source of a sharp optical resonance feature is the van Hove singularity (VHS) in the joint density of states of free electron-hole pair excitation spectrum, but this possibility cannot explain P1 because it is an absorption peak isolated from the rest of the spectrum. In terms of P2, the possibility of VHS at the band edge indeed exists in the simplest tight-binding model of bandgap-opened BLG (*3*). However, by comparing our experimentally obtained spectrum with a tight-binding model, we found that P2 is always much sharper than the peak in the theory-predicted absorption spectrum (fig. S4). When electron-electron interactions are included, the Sommerfeld factor will further broaden the VHS peak in optical absorption spectrum in 1D and 2D systems (*18, 19*). Thus, we rule out the VHS origin of both P1 and P2. Next, we examined the possibility of impurity-originated optical absorption. We measured the doping-dependent photocurrent spectrum (fig. S3) and found that both P1 and P2 are robust against finite doping of electrons and holes, whereas impurity-originated optical transitions would be forbidden by Pauli blocking as the impurity level is filled/emptied. The doping range that we have tested is one order of magnitude higher than the known lattice-defect density, but further doping is not possible in our experiment due to degraded signal-to-noise ratio (*14*). Thus, further investigations are needed to fully understand the behavior of P1 and P2 with increased doping, such as possible screening effects and other impurity-related mechanisms.

We therefore assign P1 and P2 to optical transitions to the exciton 1s state and 2p state, respectively (Fig. 3A). Although the photocurrent spectrum could differ from the absorption spectrum owing to the unknown quantum efficiency of excitons dissociating into free carriers, photocurrent spectroscopy has been widely used to understand fundamental optical resonances in semiconductors (*20, 21*). Quantitatively, the peaks in the optical absorption spectrum corresponding to P1 and P2 would be even more prominent if this quantum efficiency were corrected for, making the VHS origin even less likely. Above P2, there is a bump-like feature that can be traced as a diagonal line in Fig. 2B, similar to the trend of P1 and P2. Although it may also originate from an excitonic transition, its broad line width makes a definitive assignment impossible. In conventional semiconductors such as GaAs, the exciton s

¹Kavli Institute at Cornell for Nanoscale Science, Ithaca, NY 14853, USA. ²Laboratory of Atomic and Solid State Physics, Cornell University, Ithaca, NY 14853, USA. ³Department of Physics, University of California, Berkeley, CA 94720, USA. ⁴National Institute for Materials Science, 1-1 Namiki, Tsukuba 305-0044, Japan. ⁵Materials Sciences Division, Lawrence Berkeley National Laboratory, Berkeley, CA 94720, USA.

⁶School of Electrical and Computer Engineering, Cornell University, Ithaca, NY 14853, USA. ⁷Department of Chemistry and Chemical Biology, Cornell University, Ithaca, NY 14853, USA. ⁸Department of Mechanical Engineering, Columbia University, New York, New York 10027, USA. ⁹Kavli Energy NanoSciences Institute at the University of California, Berkeley, and the Lawrence Berkeley National Laboratory, Berkeley, CA 94720, USA.

*These authors contributed equally to this work.

†Corresponding author. Email: plm23@cornell.edu (P.L.M.); fengwang76@berkeley.edu (F.W.); jh2228@columbia.edu (J.H.)

states are optically bright, whereas the p states are dark. In BLG, because of the valley-dependent electron pseudospin winding number of 2, the electron-hole pair acquires an internal z-component angular momentum $m_{ps} = -2(+2)$ in K(K') valley (9); exciton states are additionally characterized by the angular momentum quantum number of their envelope function, m_{env} (Fig. 3A). A continuum model with full rotational symmetry around the K and K' points predicts that the exciton 1s state ($m_{env} = 0$) is dark, whereas one of exciton 2p states ($m_{env} = +1$ in K, and $m_{env} = -1$ in K' valley) is bright for normal incident radiation (9, 10). This can be understood by considering that a photon can change the total angular momentum quantum number $m = m_{ps} + m_{env}$ by ± 1 . When the direct hopping term γ_3 is included (22), the full rotation symmetry around the K and K' points will be slightly broken, and it results in the trigonal warping effect of exciton envelope function (Fig. 3B). As a result, the 1s exciton state is not completely dark. Quantitatively, our ab initio GW Bethe-Salpeter equation (GW-BSE) calculation (23) predicts that the ratio between the oscillator strength of 1s exciton and 2p exciton is

about 0.05. Experimentally, we found the ratio between oscillator strength of P1 and P2 to be ~ 0.07 to 0.08 (fig. S5), confirming the unusual selection rules.

We now further discuss the exciton binding energies. The determination of the exact value of exciton binding energy and the bandgap energy is not possible because the location of the quasiparticle bandgap is not obvious in the photocurrent spectrum. Nevertheless, $(P2 - P1)/P2$ gives a lower bound of the binding energy of exciton 1s state, whereas the ratio $(P2 - P1)/P2$ provides a lower bound of the ratio between binding energy and bandgap. For a small D , this ratio is close to 20%, much larger than in conventional semiconductors.

The pseudospin degree of freedom (DOF) also dramatically affects the magnetic properties of the excitons. Figure 4A shows photocurrent spectrum as a function of the magnetic field perpendicular to the sample plane at a fixed $D = 1.03$ V/nm. The peak P1 splits linearly with the magnetic field, corresponding to an effective gyromagnetic factor (*g*-factor) of 19.8 ± 0.1 (Fig. 4, A and B). This *g*-factor is about 5 times as large as the exciton valley

Zeeman *g*-factor in transition metal dichalcogenides (TMDCs) (24–27). The average energy of the split P1 peaks is plotted in the lower panel of Fig. 4C (P1 center). The shift of this average energy can be well fitted with quadratic term αB^2 , where $\alpha \approx 0.2$ meV T $^{-2}$. As shown in the upper panel of Fig. 4C, the peak P2 also shows a quadratic dependence on magnetic field B , with a coefficient β similar to α at small magnetic field, but its overall behavior is more complicated in the full range.

We first discuss the linear splitting (Zeeman) term of excitons in the magnetic field. In conventional semiconductors [as well as TMDCs (24–27)], the different atomic orbital nature (and thus magnetic moment) of conduction and valence bands produces the Zeeman shift. In contrast, both bands in BLG are of the p_z nature, meaning that the atomic orbital contribution to the exciton Zeeman shift is zero. The electron-spin contribution is also expected to be zero because the optically bright excitons are spin-singlet states. Instead, the electron-hole pair acquires an internal magnetic moment from the wave packet self-rotation (28) associated with the pseudospin DOF.

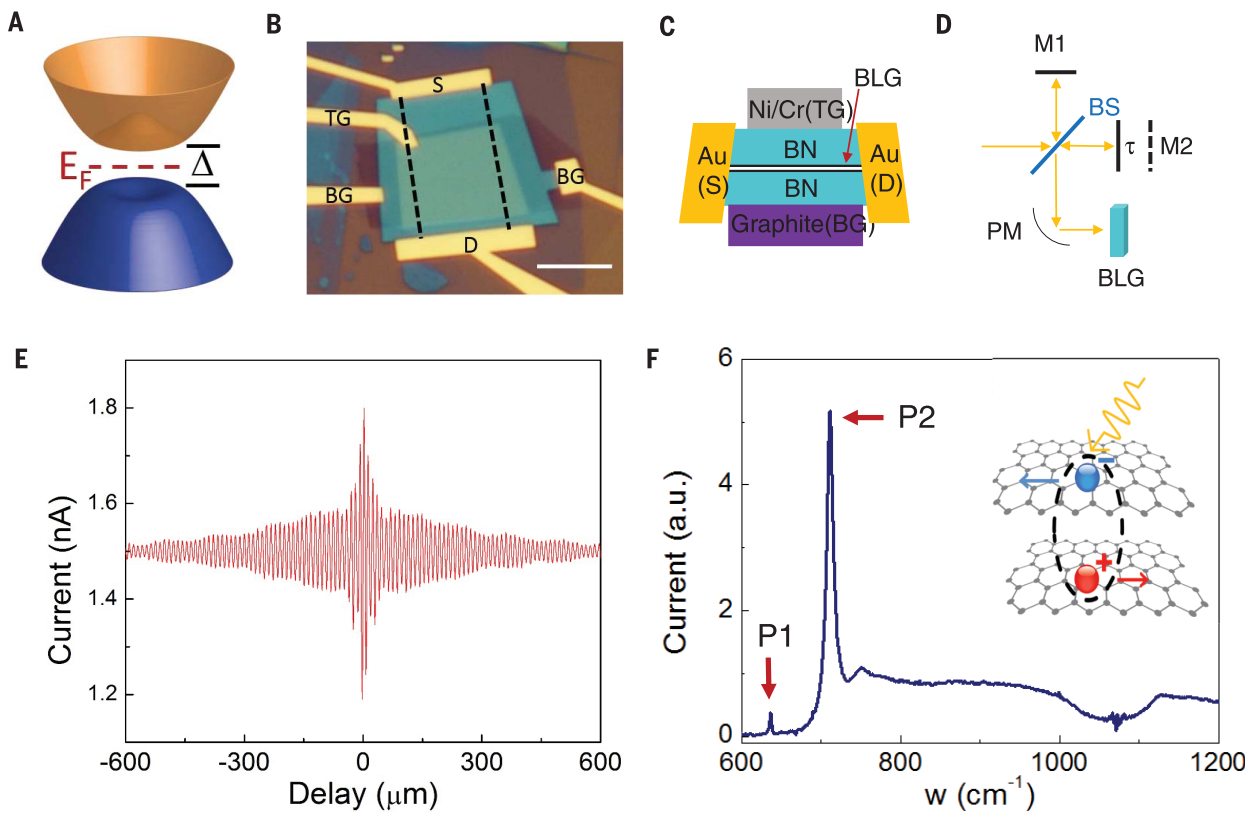


Fig. 1. Device configuration and measurement scheme. (A) The “Mexican hat” band structure of BLG with a bandgap of Δ at charge-neutral condition. (B) Optical micrograph of a dual-gated hBN-encapsulated BLG device. The graphene flake enclosed by the dashed lines is sandwiched by the graphite back gate and Ni/Cr top gate, with hBN as the dielectrics (inset shows a sketch of the cross section). Scale bar, 10 μm . (C) The cross section of the device in (B). (D) Illustration of the interferometer setup where M1, M2, BS, PM, and τ represent the static mirror, moving mirror,

beamsplitter, parabolic mirror, and delay, respectively. (E) A typical photocurrent interferogram of gapped BLG as the delay τ between two beam paths is continuously scanned. (F) Photocurrent spectrum obtained by Fourier-transforming the interferogram in (E). Two sharp peaks (P1 and P2 indicated by red arrows) are observed as the lowest energy spectrum features. The inset illustrates the photocurrent generation process. Excitons excited by incident light are dissociated into free electrons and holes and contribute to electrical current under an external electric field.

Fig. 2. Photocurrent spectrum of bandgap-tuned BLG. (A) Normalized photocurrent spectrum at displacement field $D = 0.69, 1.03$, and 1.37 V/nm [corresponding to dashed lines in (B)]. Both P1 and P2 blueshift as D increases and the bandgap opens more. All spectra converge to a line at energies above P2. (B) Two-dimensional mapping of photocurrent as a function of the displacement field and photon energy. (C) Peak energy as a function of D . Both P1 and P2 (reduced by a factor of 15 for comparison) decrease in a largely linear fashion with decreasing D , whereas $(P_2 - P_1)$ decreases nonlinearly. The ratio $(P_2 - P_1)/P_2$ increases by more than two times from $D = 1.37$ V/nm to $D = 0.34$ V/nm. (D) Fittings of P1 and P2 at $D = 1.03$ V/nm. P1 is fitted with a Lorentzian line shape with a FWHM of 0.4 meV, and P2 is well described by a Lorentzian line shape with a FWHM of 1.3 meV.

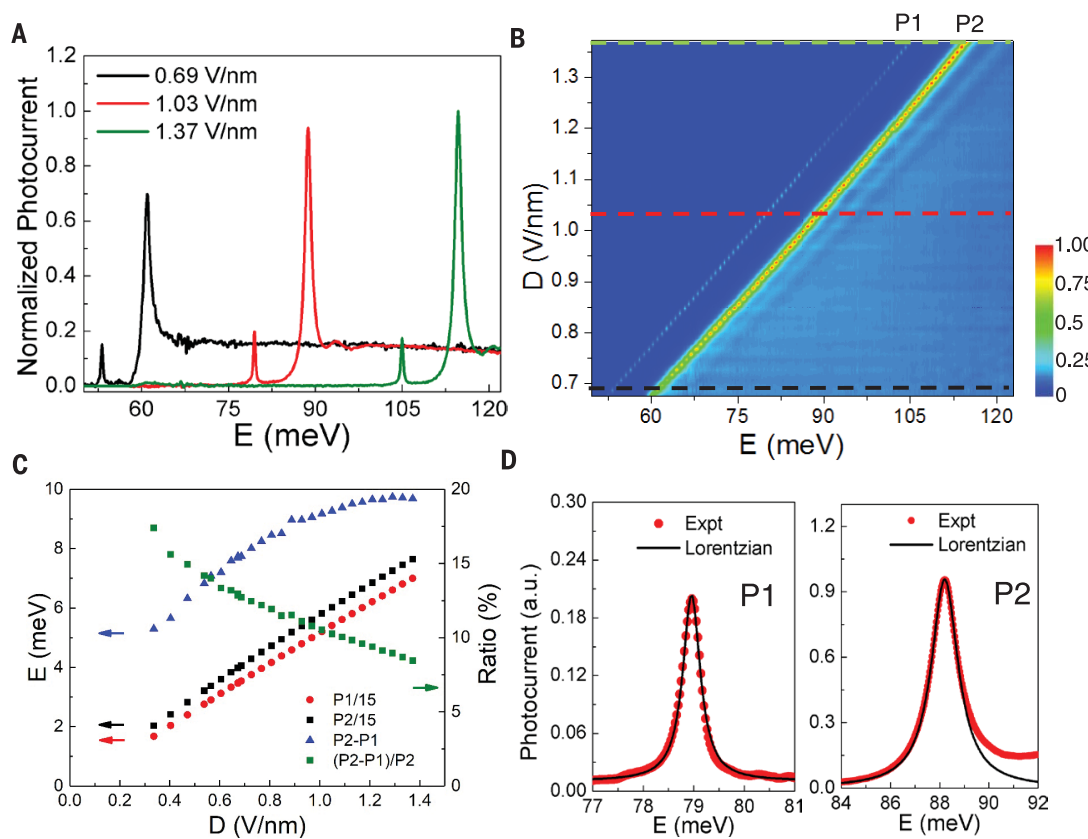
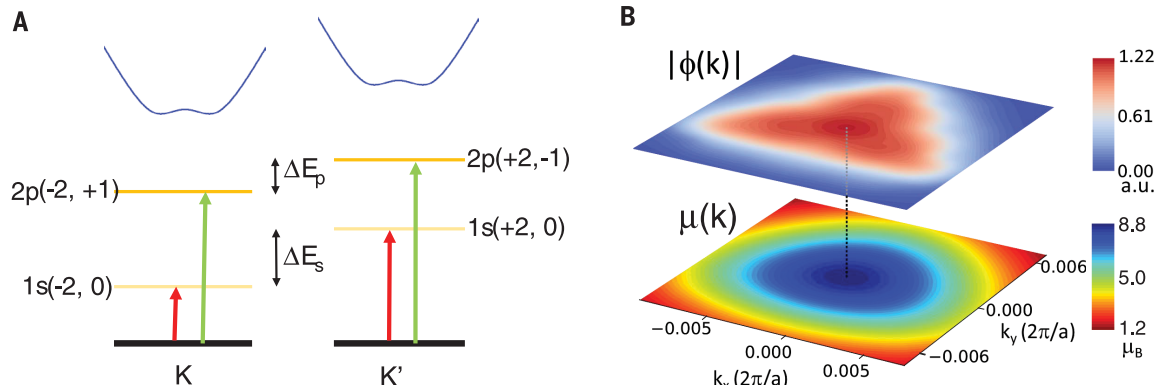


Fig. 3. Theoretical understanding of the origin of P1 and P2. (A) Valley-dependent selection rules and valley splitting of excitons in gapped BLG. Black and blue lines represent ground state and free electron-hole pair states. Exciton states are labeled by m_{ps} (the quantum number of pseudospin angular momentum) and m_{env} (the quantum number of exciton envelope function angular momentum). The optical selection rules are distinct from those in conventional semiconductors, because of the electron pseudospin winding number of 2: Transitions from the ground state to the exciton 1s state are forbidden under rotational symmetry and are barely allowed in real BLG; optical transitions to 2p states ($m_{env} = +1$ in K valley and $m_{env} = -1$ in K' valley) are allowed, and they take most of the oscillator strength. Valley splitting of the exciton energy levels ΔE_s and ΔE_p can be induced by applying a



magnetic field. (B) Momentum-resolved envelope function of the exciton 1s state (upper panel) and asymmetric magnetic moment of single-particle electron-hole pair states (lower panel) in K valley based on ab initio GW-BSE calculation (14). The origin (0, 0) corresponds to K. The $\mu(k)$ in K' valley is opposite of that in K valley. The magnetic moment of 1s exciton [$\mu(k)$] weighted by $|\phi(k)|^2$ is $6.4 \mu_B$, which results in a valley splitting of $12.8 \mu_B$, comparable to the $19.8 \mu_B$ observed experimentally.

This magnetic moment originates purely from the orbital DOF, and it is a manifestation of the Berry curvature effect. This magnetic moment shifts the electron and hole bands around a given valley equally if there is perfect electron-hole

symmetry (29), but BLG has a finite band asymmetry (30–32), resulting in an effective magnetic moment of an optically excited single-particle electron-hole pair. Such magnetic moments have opposite signs in K and K' valleys and cause a

valley Zeeman splitting of excitons. We plot the calculated effective magnetic moment μ_{ps} as in the K valley at $D = 1.03$ V/nm for single-particle electron-hole pairs in the bottom panel of Fig. 3B and obtain an effective $g = 6.4$ for exciton 1s state.

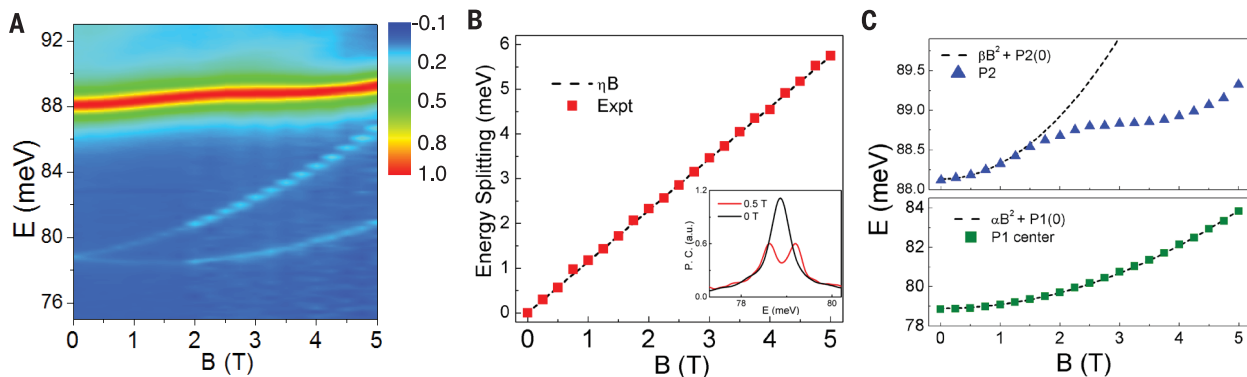


Fig. 4. Magnetic field dependence of exciton transitions. (A) Normalized photocurrent spectrum for $D = 1.03 \text{ V/nm}$ as a function of magnetic field. P1 splits into two peaks, whereas the splitting of P2 is not discernible. (B) Energy splitting of P1 as a function of magnetic field extracted from (A). The splitting scales linearly with B with a coefficient η of 1.15 meV T^{-1} , 19.8 ± 0.1 times the Bohr magneton. The inset shows photocurrent spectra at 0 T and 0.5 T . The 0.5 T spectrum clearly shows the separation of the two 1s valley excitons as a result of the large g -factor. (C) Dependence

of the average energy of the split P1 peaks (bottom panel) and the P2 energy (upper panel) on magnetic field. The former can be fitted with αB^2 (the dashed line) with $\alpha = 0.2 \text{ meV T}^{-2}$, corresponding to the diamagnetism of an S exciton with a radius of $\sim 6 \text{ nm}$. The P2 energy at $B < 2 \text{ T}$ can be fitted by βB^2 (the dashed line), where β has a similar value to α . A more complete model that includes both excitons and transitions between Landau levels is needed to explain the behavior of P2 in the full range of the magnetic field.

This corresponds to a valley splitting of $g = 12.8$, comparable to the experimentally extracted value of 19.8.

The quadratic dependence on B of the averaged P1 energy corresponds to the diamagnetism effect (33, 34) of excitons. Semiclassically, the diamagnetic coefficient of exciton can be expressed as: $\frac{e^2}{8\mu}\langle r^2 \rangle$, where μ is the reduced mass of exciton and $\langle r^2 \rangle$ characterizes the size of exciton orbit. However, in the “Mexican hat” band structure of bandgap-opened BLG (Fig. 1A), the electrons and holes near the band edge cannot be described by a single effective mass and no quantitative theory is available. We can roughly estimate the exciton radius by assuming a reduced mass of $\mu = \frac{\Delta}{4v_F^2}$ (where $\frac{\Delta}{2v_F^2}$ is approximately the rest mass of elec-

tron given a bandgap of Δ and a Fermi velocity of v_F). For $\Delta = 0.1 \text{ eV}$, we obtained a radius of 1s exciton to be $\sim 6 \text{ nm}$.

The large valley-splitting g -factor, together with the narrow line width of 1s excitons, makes it easy to break the valley degeneracy in BLG. As shown by the inset of Fig. 4B, a magnetic field as low as 0.5 T (achievable by a permanent magnet) can separate the two valley excitons in energy. This effect offers a convenient way of controlling the valley DOF by resonant optical excitation, therefore enabling valley-dependent optical and optoelectronic studies in graphene (35), as well as their applications for valleytronics. This, combined with the electrostatic tunability, makes BLG a particularly good material system for various optical and optoelectronic applications such as tunable infrared detectors, light-emitting diodes, and lasers.

The results reported here offer many challenges to theorists. In the case of the 2p exciton in BLG, no theory exists for the Zeeman effect, although the orbital splitting should oppose the pseudospin splitting (14). Experimentally, a magnetic-field-induced splitting is not seen (smaller than 20% of the line width of the 2p exciton transi-

tion). Similarly, no quantitative theory exists for the observed diamagnetic (quadratic) shifts of the P1 exciton with the magnetic field or the more complex behavior seen for P2. Because the 2p exciton is closer to the quasiparticle band edge, its complicated behavior at fields above 2 T might be a consequence of interactions with the lowest Landau-level transition. A more systematic study in this direction could lead to an improved understanding of interactions between excitons and Landau-level transitions.

REFERENCES AND NOTES

- Y. Zhang et al., *Nature* **459**, 820–823 (2009).
- E. V. Castro et al., *Phys. Rev. Lett.* **99**, 216802 (2007).
- E. McCann, *Phys. Rev. B* **74**, 161403 (2006).
- H. K. Min, B. Sahu, S. K. Banerjee, A. H. MacDonald, *Phys. Rev. B* **75**, 155115 (2007).
- J. B. Oostinga, H. B. Heersche, X. Liu, A. F. Morpurgo, L. M. K. Vandersypen, *Nat. Mater.* **7**, 151–157 (2008).
- C.-H. Park, N. Marzari, *Phys. Rev. B* **84**, 205440 (2011).
- K. S. Novoselov et al., *Nat. Phys.* **2**, 177–180 (2006).
- F. Zhang, J. Jung, G. A. Fiete, Q. Niu, A. H. MacDonald, *Phys. Rev. Lett.* **106**, 156801 (2011).
- C. H. Park, S. G. Louie, *Nano Lett.* **10**, 426–431 (2010).
- V. V. Cheianov, I. L. Aleiner, V. I. Fal’ko, *Phys. Rev. Lett.* **109**, 106801 (2012).
- B. Stuart, *Infrared Spectroscopy* (Wiley Online Library, 2005).
- L. Wang et al., *Science* **342**, 614–617 (2013).
- M. Vanecak, A. Poruba, *Appl. Phys. Lett.* **80**, 719–721 (2002).
- See additional text and data in the supplementary materials.
- J. Tomm, K. Herrmann, A. Yunovich, *Phys. Status Solidi* **122**, 11–42 (1990).
- D. S. L. Abergel, V. I. Fal’ko, *Phys. Rev. B* **75**, 155430 (2007).
- E. J. Nicol, J. P. Carbotte, *Phys. Rev. B* **77**, 155409 (2008).
- T. Ogawa, T. Takagahara, *Surf. Sci.* **263**, 506–511 (1992).
- M. Shinada, S. Sugano, *J. Phys. Soc. Jpn.* **21**, 1936–1946 (1966).
- R. T. Collins, K. Klitzing, K. Ploog, *Phys. Rev. B Condens. Matter* **33**, 4378–4381 (1986).
- K. F. Mak, C. Lee, J. Hone, J. Shan, T. F. Heinz, *Phys. Rev. Lett.* **105**, 136805 (2010).
- M. S. Dresselhaus, G. Dresselhaus, *Adv. Phys.* **51**, 1–186 (2002).
- M. Rohlfing, S. G. Louie, *Phys. Rev. B* **62**, 4927–4944 (2000).
- D. MacNeill et al., *Phys. Rev. Lett.* **114**, 037401 (2015).
- G. Avizian et al., *Nat. Phys.* **11**, 148–152 (2015).
- A. Srivastava et al., *Nat. Phys.* **11**, 141–147 (2015).
- Y. Li et al., *Phys. Rev. Lett.* **113**, 266804 (2014).
- M.-C. Chang, Q. Niu, *Phys. Rev. B Condens. Matter* **53**, 7010–7023 (1996).
- D. Xiao, W. Yao, Q. Niu, *Phys. Rev. Lett.* **99**, 236809 (2007).
- L. M. Zhang et al., *Phys. Rev. B* **78**, 235408 (2008).
- E. A. Henriksen et al., *Phys. Rev. Lett.* **100**, 087403 (2008).
- K. Zou, X. Hong, J. Zhu, *Phys. Rev. B* **84**, 085408 (2011).
- S. N. Walck, T. L. Reinecke, *Phys. Rev. B* **57**, 9088–9096 (1998).
- K. J. Nash, M. S. Skolnick, P. A. Claxton, J. S. Roberts, *Phys. Rev. B Condens. Matter* **39**, 10943–10954 (1989).
- W. Yao, D. Xiao, Q. Niu, *Phys. Rev. B* **77**, 235406 (2008).

ACKNOWLEDGMENTS

We acknowledge H. Wang, R. Frinks, and O. Koksal for help with FTIR measurement. L.J. and L.W. acknowledge support from a Kavli Postdoctoral Fellowship. The work at Cornell was supported in part by the Cornell Center for Materials Research, with funding from NSF’s Materials Research Science and Engineering Center program (DMR-1120296); by the Nanoelectronics Research Corporation (NERC), a wholly owned subsidiary of the Semiconductor Research Corporation (SRC); through the Institute for Nanoelectronics Discovery and Exploration (INDEX); by the Air Force Office of Scientific Research (MURI: FA9550-16-1-0031); and by the Office of Naval Research under grant no. N00014-12-1-0072. Sample fabrication was performed at the Cornell Nanoscale Science and Technology Facility, a member of the National Nanotechnology Infrastructure Network, which is supported by NSF (ECCS-1542081). Measurements and theoretical and computational work at the Lawrence Berkeley National Laboratory (LBNL) were supported by the Center for Computational Study of Excited-State Phenomena in Energy Materials at LBNL, which is funded by the U.S. Department of Energy (DOE), Office of Science, Basic Energy Sciences, Materials Sciences and Engineering Division, under contract no. DE-AC02-05CH11231, as part of the Computational Materials Sciences Program. Computational resources were provided by DOE at LBNL’s National Energy Research Scientific Computing Center facility.

SUPPLEMENTARY MATERIALS

www.sciencemag.org/content/358/6365/907/suppl/DC1
Materials and Methods
Supplementary Text
Figs. S1 to S7
References (36–40)

5 February 2017; accepted 5 October 2017
10.1126/science.aam9175

Tunable excitons in bilayer graphene

Long Ju, Lei Wang, Ting Cao, Takashi Taniguchi, Kenji Watanabe, Steven G. Louie, Farhan Rana, Jiwoong Park, James Hone, Feng Wang and Paul L. McEuen

Science 358 (6365), 907-910.
DOI: 10.1126/science.aam9175

Pairing up electrons and holes in bilayer graphene

Excitons—bound pairs of electron and holes in solids—can be harnessed for optoelectronic applications. Being able to tune the exciton energy would bring functional flexibility to such devices. Although tunable excitons have been predicted to form in bilayer graphene, observing them experimentally has been difficult. Ju *et al.* used high-quality bilayer graphene samples sandwiched between layers of hexagonal boron nitride to observe excitons in this material. Exciton energy was tuned across a large range by controlling the gate voltages.

Science, this issue p. 907

ARTICLE TOOLS

<http://science.scienmag.org/content/358/6365/907>

SUPPLEMENTARY MATERIALS

<http://science.scienmag.org/content/suppl/2017/11/16/358.6365.907.DC1>

REFERENCES

This article cites 38 articles, 1 of which you can access for free
<http://science.scienmag.org/content/358/6365/907#BIBL>

PERMISSIONS

<http://www.scienmag.org/help/reprints-and-permissions>

Use of this article is subject to the [Terms of Service](#)